JEM Journal of Experimental Medicine

ARTICLE

TGFβ signaling in germinal center B cells promotes the transition from light zone to dark zone

Anne R. Albright[1], Juraj Kabat[2], Moyi Li[1], Fiona Raso[3], Andrea Reboldi[3], and Jagan R. Muppidi[1]

B cells in germinal centers (GCs) cycle between light zone (LZ) and dark zone (DZ). The cues in the GC microenvironment that regulate the transition from LZ to DZ have not been well characterized. In Peyer's patches (PPs), transforming growth factor-β (TGFβ) promotes IgA induction in activated B cells that can then differentiate into GC B cells. We show here that TGFβ signaling occurs in B cells in GCs and is distinct from signaling that occurs in activated B cells in PPs. Whereas in activated B cells TGFβ signaling is required for IgA induction, in the GC it was instead required for the transition from LZ to DZ. In the absence of TGFβ signaling, there was an accumulation of LZ GC B cells and reduced antibody affinity maturation likely due to reduced activation of Foxo1. This work identifies TGFβ as a microenvironmental cue that is critical for GC homeostasis and function.

Introduction

Germinal centers (GCs) form in secondary lymphoid organs following immunization and after infection and are necessary for humoral immunity to pathogens (Victora and Nussenzweig, 2012). B cells in GCs cycle between the light zone (LZ), where they can receive T cell help on the basis of their ability to acquire antigen via their B cell receptor (BCR), and the dark zone (DZ), where they proliferate and undergo somatic hypermutation of their BCR (Victora and Nussenzweig, 2012). Iterative cycling of GC B cells (GCBs) between LZ and DZ allows for the generation of B cells expressing high-affinity BCR. Recent work has demonstrated that the transcription factor forkhead box protein O1 (Foxo1) is required for GCBs to maintain the DZ state (Dominguez-Sola et al., 2015; Sander et al., 2015; Inoue et al., 2017). Foxo1 was shown to be more active in DZ GCBs. In the LZ, Foxo1 is phosphorylated (p), preventing it from entering the nucleus and targeting it for degradation. A fraction of LZ GCBs show active nuclear Foxo1, and these cells are thought to be in the process of transitioning to the DZ (Sander et al., 2015). While BCR signaling has been implicated in inducing the phosphorylation of Foxo1, the cues in the GC microenvironment that might induce dephosphorylation and nuclear translocation of Foxo1 in LZ cells and allow for transition to the DZ state have not been defined (Cyster, 2015; Luo et al., 2018).

In mucosal lymphoid tissue such as Peyer's patches (PPs) and mesenteric LNs (mLNs), GCs are thought to form in response to chronic stimulation by microbial products and other stimuli derived from the gut (Fagarasan et al., 2010; Reboldi and Cyster, 2016). PPs are key sites for induction of IgA, which is the most abundant Ig in the body and is important for maintenance of homeostasis of the gut microbiota and defense against enteric pathogens. PPs can be divided into distinct areas: (1) the B cell follicle, which consists primarily of naive B cells and also contains GCs; (2) the follicle-associated epithelium (FAE), which overlies with PPs on the luminal side of the gut; (3) the subepithelial dome (SED), which lies between the follicle and the FAE and is enriched in dendritic cells (DCs); and (4) interfollicular areas that contain T cells and DCs (Reboldi and Cyster, 2016; Lycke and Bemark, 2017). Recent work has shown that before differentiation into GCBs, activated IgD$^+$ pre-GCBs up-regulate the chemokine receptor Ccr6 and migrate into the SED in a Ccr6-dependent fashion, where they interact with DCs. Class switch recombination (CSR) to IgA is initiated in activated IgD$^+$ pre-GC cells (Reboldi et al., 2016). SED DCs are thought to promote induction of IgA in activated B cells via integrins that activate TGFβ from its latent form (Reboldi et al., 2016). However, it has not been directly demonstrated that TGFβ signaling occurs in activated pre-GCBs in the SED in situ. It has also been proposed that other cells in PPs, such as follicular DCs (FDCs), may provide active TGFβ to GCBs (Suzuki et al., 2010). Whether TGFβ signaling occurs in PP GCBs or GCBs in nonmucosal sites has not

[1]Lymphoid Malignancies Branch, Center for Cancer Research, National Cancer Institute, National Institutes of Health, Bethesda, MD; [2]Biological Imaging Section, Research Technologies Branch, National Institute of Allergy and Infectious Diseases, National Institutes of Health, Bethesda, MD; [3]Department of Pathology, University of Massachusetts Medical School, Worcester, MA.

Correspondence to Jagan R. Muppidi: jagan.muppidi@nih.gov.

been demonstrated in situ; nor is it clear what role TGFβ signaling in GCBs might play in IgA induction or GC homeostasis.

TGFβ is a pleiotropic cytokine that is secreted in an inactive form and can be activated when integrins bind to the latency-associated peptide and release active TGFβ (Travis and Sheppard, 2014). Active TGFβ can then bind to Tgfbr2 homodimers, which then form a complex with a homodimer of Tgfbr1. This tetrameric complex can then recruit and phosphorylate Smad2 or Smad3 proteins. pSmad2/3 can then interact with other proteins such as Smad4 and enter the nucleus where this complex can regulate gene expression (Travis and Sheppard, 2014; David and Massagué, 2018). In addition to Smad-dependent signaling, TGFβ can also signal independently of Smad via a number of different pathways. For example, in hematopoietic stem cells, TGFβ has been reported to promote the nuclear translocation of Foxo3 (Yamazaki et al., 2009; Naka et al., 2010).

TGFβ strongly promotes the induction of IgA as B cell–specific loss of Tgfbr2 leads to near complete loss of IgA (Cazac and Roes, 2000). In addition to loss of IgA, B cell–specific loss of Tgfbr2 was also reported to result in hyperplasia of PPs with increased GCs (Cazac and Roes, 2000). However, in the absence of Ccr6, where access of activated B cells to TGFβ in the SED is reduced, there is a reduction in IgA, but outgrowths of Ccr6-deficient PP GCBs have not been reported (Reboldi et al., 2016).

In this study, we sought to determine with high resolution the sites of TGFβ signaling in situ. We provide confirmation that rare IgD$^+$ B cells in the SED in PPs contain pSmad2; however, we also found that GCBs in mucosal as well as nonmucosal sites showed evidence of TGFβ signaling. We found that in the absence of Tgfbr1 in all mature B cells there was a loss of IgA, while when Tgfbr1 was lost in GCBs, CSR to IgA could still occur. In both models, there was a cell-intrinsic expansion of mucosal GCBs, most prominently in PP GCs, and an increase in LZ phenotype cells in both mucosal and nonmucosal GCs likely as a result of reduced activation of Foxo1. Additionally, we found that TGFβ signaling in GCs promoted antibody affinity maturation. Finally, we demonstrated that FDCs are required to promote TGFβ signaling in GCBs. This work identifies TGFβ signaling in GCBs as an important microenvironmental cue that supports GC polarity in both mucosal and nonmucosal sites that is distinct from its role in supporting IgA induction.

Results

TGFβ signaling occurs in GCBs and IgD$^+$ B cells in the SED

Activated pre-GCBs up-regulate Ccr6, which guides the cells to the Ccl20-rich SED in PPs (Reboldi et al., 2016; Nagashima et al., 2017). TGFβ signaling is thought to promote IgA induction in activated pre-GCBs in the SED of PPs. Ligation of TGFβ receptors results in the phosphorylation of Smad2 or Smad3. Therefore, we sought to determine whether TGFβ signaling occurs in B cells in the SED by performing immunofluorescence of pSmad2 in PPs. The SED is an area between the FAE and the follicle and is enriched in CD11c$^+$ DCs. We could identify rare IgD$^+$ cells in the SED that were pSmad2$^+$ (Fig. 1 A). In addition to the rare IgD$^+$ pSmad2$^+$ cells in the SED, anti-pSmad2 staining was prominent in PP GCs (Fig. 1, A and B). We also stained PPs from *Cr2-cre Tgfbr1$^{f/f}$* mice in which Tgfbr1 is deleted in mature B cells. In the absence of Tgfbr1 in mature B cells, we saw decreased pSmad2 staining in the GC and were unable to find IgD$^+$ cells in the SED that stained positive for pSmad2 (Fig. 1 B and image analysis below).

Given the known role of TGFβ signaling in the SED, we asked whether TGFβ signaling in the GC is independently initiated and has unique outcomes. Although activation-induced cytidine deaminase (AID) is expressed at low levels in IgD$^+$ pre-GCBs in the SED (Reboldi et al., 2016), we reasoned that this low level of AID expression in pre-GCBs would not be sufficient to allow for complete deletion of two copies of a floxed gene when Cre is expressed under the control of the *Aicda* locus. Therefore, to assess the GC-specific functions of TGFβ signaling, we crossed *Aicda$^{cre/+}$* animals to *Tgfbr1* floxed animals. We analyzed pSmad2 in PPs from *Aicda$^{cre/+}$ Tgfbr1$^{f/f}$* animals and found that pSmad2 could be seen in IgD$^+$Bcl6$^-$ cells in the SED but was strongly reduced in the GC compared with *Aicda$^{cre/+}$ Tgfbr1$^{f/+}$* animals (Fig. 1 C and image analysis below). To quantify TGFβ signaling in PP B cells, we performed histocytometry (Gerner et al., 2012; Radtke et al., 2015). Histocytometry imaging analysis allows for quantification of fluorescence in multiple parameters on a per-cell basis. We stained PPs with the nucleic acid stain JoPro-1 to mark nuclei and antibodies specific for B220, IgD, Bcl6, CD11c, and pSmad2. We used CD11c and IgD staining to define the SED and follicle, respectively. Within each of these areas, we gated on B cells using B220. Within the B cell gate in the follicle, we were able to identify naive B cells that were IgD$^+$ Bcl6$^-$ and GCBs that were IgD^{lo}Bcl6$^+$ (Fig. 1 D). In GCBs, we observed strong pSmad2 activity compared with IgD$^+$ cells in the follicle (Fig. 1, D and E). We found that IgD$^+$ B cells could be identified in the SED of PPs, and that rare IgD$^+$ B cells that were also pSmad2$^+$ could be identified (Fig. 1, D and E). Importantly, pSmad2$^+$ cells were strongly reduced in GCBs and IgD$^+$ cells in the SED of PPs of *Cr2-cre Tgfbr1$^{f/f}$* animals (Fig. 1 E). *Aicda$^{cre/+}$ Tgfbr1$^{f/f}$* animals showed reduced pSmad2 activity in the GC at levels comparable to *Cr2-cre Tgfbr1$^{f/f}$* animals (Fig. 1 E). However, pSmad2$^+$ IgD$^+$ cells in the SED were only partially reduced in *Aicda$^{cre/+}$ Tgfbr1$^{f/f}$* animals in contrast to *Cr2-cre Tgfbr1$^{f/f}$* animals (Fig. 1 E). These data show that in addition to the expected location of TGFβ signaling in activated pre-GCBs in the SED of the PPs, evidence of active TGFβ signaling can be seen in PP GCBs.

As an additional test of whether access to the SED by activated IgD$^+$ pre-GCBs was related to or distinct from TGFβ signaling in the GC, we assessed TGFβ signaling in Ccr6-deficient GCBs. Ccr6 is up-regulated on activated pre-GC cells and promotes migration to the SED, where they can interact with DCs and receive TGFβ stimulation (Reboldi et al., 2016). Because Ccr6–fully deficient animals lack a developed SED and have reduced GC activity, we generated mixed bone marrow chimeras by reconstituting irradiated CD45.1 hosts with WT or Ccr6-deficient bone marrow that was CD45.2 mixed with WT CD45.1 bone marrow. We assessed pSmad2 in PP GCs of these chimeras by immunofluorescence. In addition to pSmad2, we co-stained sections for IgD, CD45.2, Bcl6, and the nuclear marker JoPro-1 and analyzed these images by histocytometry. We found

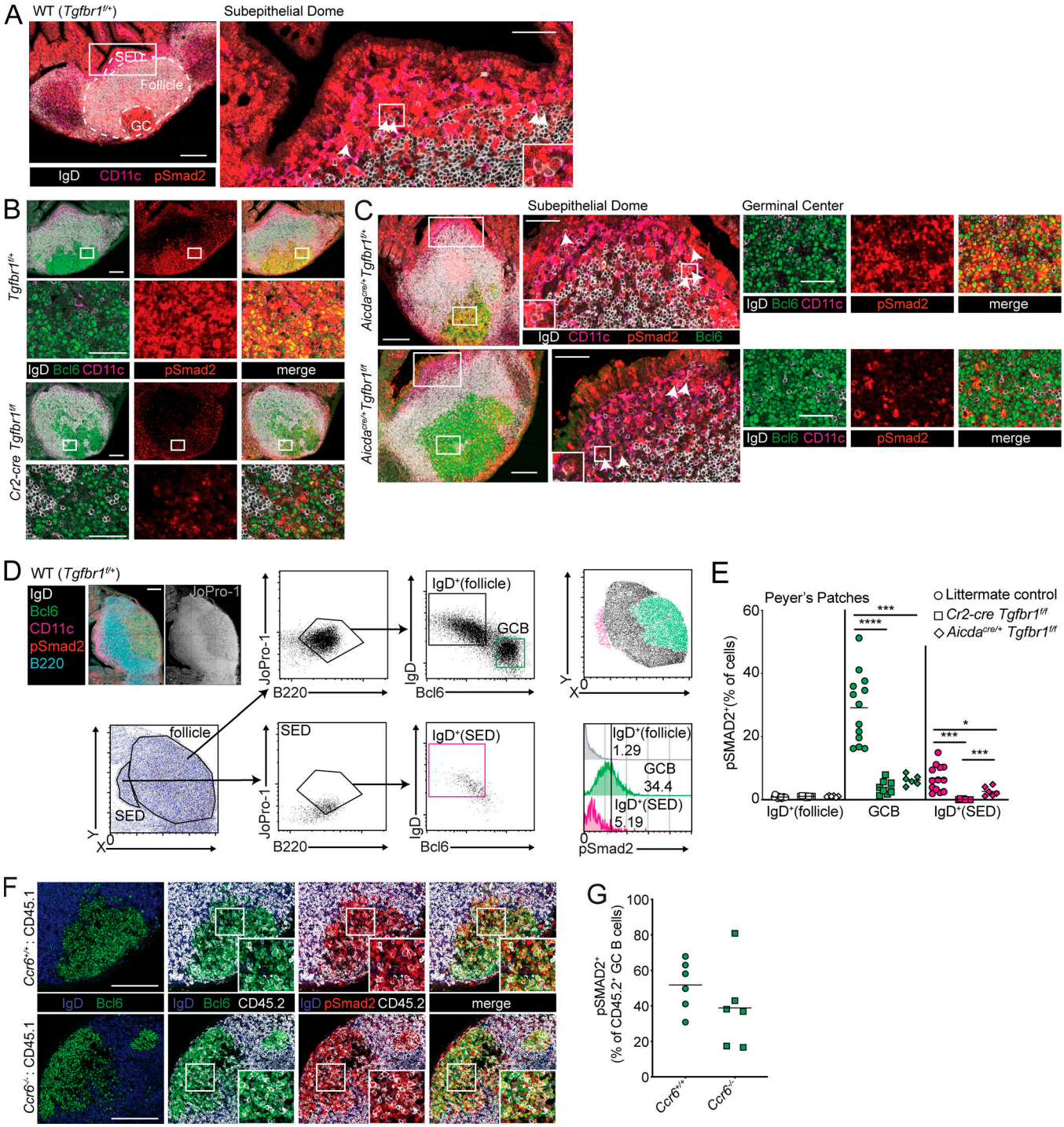

Figure 1. **TGFβ signaling occurs in PP GCBs in addition to activated IgD⁺ B cells in the SED. (A)** Confocal microscopy of PPs from a WT (*Tgfbr1*$^{f/+}$) animal stained for IgD (white), CD11c (magenta), and pSmad2 (red). The left image shows maximal intensity projection of confocal stack. Follicle is defined by B220 staining (not shown), GC is defined by Bcl6 staining (not shown), and SED is defined by areas below the epithelium enriched for CD11c staining. The right image shows single confocal slice of SED, and arrows indicate IgD⁺ B cells positive for pSmad2, with inset of a cluster of IgD⁺ pSmad2⁺ cells in the SED. Scale bars: 150 µm (left) or 50 µm (right). Images are representative of five independent experiments with a total of five mice. **(B)** Confocal microscopy of PPs from *Tgfbr1*$^{f/+}$ or *Cr2-cre Tgfbr1*$^{f/f}$ animals stained for IgD (white), Bcl6 (green), CD11c (magenta), and pSmad2 (red). Images of whole PPs are confocal stacks, and insets of GC are confocal slices. Scale bars: 150 µm in images of whole PPs and 50 µm in insets of GC. Images are representative of three independent experiments with a total of three mice per group. **(C)** Confocal microscopy of PPs from *Aicda*$^{cre/+}$ *Tgfbr1*$^{f/+}$ or *Aicda*$^{cre/+}$ *Tgfbr1*$^{f/f}$ animals stained for IgD (white), Bcl6 (green), CD11c (magenta), and pSmad2 (red). Left images show maximal intensity projection of confocal stack. Center images show single confocal slice of SED, and arrows indicate IgD⁺ B cells positive for pSmad2, with inset of clusters of IgD⁺ pSmad2⁺ B cells. Right images are confocal slices of GC areas. Scale bars: 150 µm (left) or 50 µm (center and right). Images are representative of two independent experiments with a total of two mice per group. **(D)** Representative histocytometry scatter plots showing gating of IgD⁺ B cells in the follicle, GCBs and IgD⁺ B cells in the SED, and histograms of pSmad2 staining in each of these populations. Scale bar: 150 µm. **(E)** Percentage of IgD⁺ B cells in follicle and GCBs or IgD⁺ B cells in the SED staining positive for pSmad2⁺ in littermate

control or *Cr2-cre Tgfbr1*$^{f/f}$ or *Aicda*$^{cre/+}$ *Tgfbr1*$^{f/f}$ mice quantified by histocytometry. Data in E are pooled data from one to four PPs per mouse from six, four, and two mice. Each dot represents one PP. **(F)** Confocal microscopy of PPs from mixed chimeras generated with 50% WT (CD45.1) BM or 50% CD45.2 BM that was *Ccr6*$^{+/+}$ or *Ccr6*$^{-/-}$ in CD45.1 hosts stained for IgD (blue), Bcl6 (green), CD45.2 (white), and pSmad2 (red). Scale bars: 150 µm. Data are representative of three mice of each type. **(G)** Percentage of pSmad2$^+$ cells among CD45.2$^+$ GCBs in PPs of mixed chimeras quantified by histocytometry. Data are pooled from two PPs per mouse from three mice of each type from two independent experiments. Each dot represents one PP. *, P < 0.05; ***, P < 0.001; ****, P < 0.0001; unpaired two-tailed Student's *t* test.

that pSmad2 was detectable in GCBs derived from Ccr6-deficient bone marrow (Fig. 1, F and G). These data show that TGFβ signaling in PP GCs is not dependent on access to the SED and is independently initiated in the GC.

TGFβ signaling in the PP GC suppresses the accumulation of LZ B cells

Hyperplasia of PP GCs in addition to loss of IgA has been previously reported in animals with B cell–specific deletion of Tgfbr2 (Cazac and Roes, 2000). However, in the absence of Ccr6, where access to TGFβ in the SED is reduced, IgA is reduced, but outgrowths of GCBs have not been reported (Reboldi et al., 2016). To examine the consequences of loss of TGFβ signaling in B cells in the SED versus the GC, we generated mixed bone marrow chimeras by reconstituting irradiated CD45.1 hosts with bone marrow from *Cr2-cre Tgfbr1*$^{f/f}$ or *Aicda*$^{cre/+}$ *Tgfbr1*$^{f/f}$ or littermate control animals (*Tgfbr1*$^{f/+ \text{ or } f/f}$ or *Aicda*$^{cre/+}$ *Tgfbr1*$^{f/+}$, respectively) that were CD45.2 mixed with bone marrow from WT CD45.1/2 animals in an ∼30:70 ratio. In *Cr2-cre Tgfbr1*$^{f/f}$ mixed chimeras, where TGFβ signaling is lost in both the SED and GC, we found that there was a striking increase in GCBs compared with naive follicular B cells (FoBs) derived from the Tgfbr1-deficient donor in PPs (Fig. 2 A). Importantly, in *Aicda*$^{cre/+}$ *Tgfbr1*$^{f/f}$ mixed chimeras, where TGFβ signaling is strongly reduced in the GC, we also saw an outgrowth of PP GCs (Fig. 2 B). The increase in PP GCBs was not related to irradiation as intact *Aicda*$^{cre/+}$ *Tgfbr1*$^{f/f}$ animals also showed increased PP GCBs compared with control animals (Fig. 2 C). The accumulation of Tgfbr1-deficient GCBs in PP GCs was not due to increased proliferation, as there was less BrdU incorporation in Tgfbr1-deficient GCBs compared with WT counterparts in the same chimeras (Fig. 2 D). We assessed active caspase-3 in PP GCBs from mixed chimeras directly ex vivo and found that fewer Tgfbr1-deficient GCBs were undergoing apoptosis compared with WT GCBs (Fig. 2 E).

GCBs cycle between LZ and DZ. LZ GCBs can be positively selected by T cells on the basis of their ability to acquire and present antigen and are directed to migrate to the DZ, where they can undergo multiple rounds of cell division depending on the strength of positive signals received in the LZ (Victora et al., 2010; Bannard et al., 2013; Gitlin et al., 2014). Given that Tgfbr1-deficient GCBs showed reduced proliferation, we hypothesized that this may be due to an alteration in the frequency of LZ and DZ cells. We analyzed PPs from *Cr2-cre Tgfbr1*$^{f/f}$ and *Aicda*$^{cre/+}$ *Tgfbr1*$^{f/f}$ mice and littermate controls and found that there was an expanded LZ on the basis of CD35 staining (Fig. 2, F and G). In *Cr2-cre Tgfbr1*$^{f/f}$ mice, we also found that FDCs and GCBs could be found extending well into the follicle, resulting in a disrupted appearance of the GC LZ. In *Cr2-cre Tgfbr1*$^{f/f}$ mixed BM chimeras there were increased Tgfbr1-deficient LZ GCBs in the PPs both by percentage of LZ cells and as a ratio of the frequencies of LZ to DZ cells (Fig. 2, H and I). In *Aicda*$^{cre/+}$ *Tgfbr1*$^{f/f}$ animals there was an increase in the area of the GC that was LZ as defined by CD35 staining and in the frequency of LZ GCBs in intact animals and in mixed chimeras (Fig. 2, J–M). These data suggest that TGFβ signaling in GCBs in PP GCs suppresses the accumulation of LZ GCBs in a cell-intrinsic fashion.

TGFβ signaling in GCBs is not required for IgA induction

Access to active TGFβ presented by DCs in the SED by activated pre-GCBs is critical for induction of IgA in PPs (Reboldi et al., 2016). However, it is not known whether TGFβ signaling in GCBs is required for induction of IgA. To examine the consequences of loss of TGFβ signaling in B cells in the SED versus the GC on IgA induction, we stained for IgA on GCBs in *Cr2-cre Tgfbr1*$^{f/f}$ or *Aicda*$^{cre/+}$ *Tgfbr1*$^{f/f}$ mixed chimeras. In *Cr2-cre Tgfbr1*$^{f/f}$ mixed chimeras, where TGFβ signaling is lost in both the SED and GC, we found that IgA was lost in PP GCBs derived from *Cr2-cre Tgfbr1*$^{f/f}$ bone marrow, in agreement with the known function of TGFβ signaling in induction of IgA (Fig. 3 A). In contrast, in *Aicda*$^{cre/+}$ *Tgfbr1*$^{f/f}$ mixed chimeras, where TGFβ signaling is lost in GCBs but can still occur in IgD$^+$ B cells in the SED, we found that IgA was induced in *Aicda*$^{cre/+}$ *Tgfbr1*$^{f/f}$ PP GCBs at levels comparable to *Aicda*$^{cre/+}$ *Tgfbr1*$^{f/+}$ GCBs (Fig. 3 B). Previous studies have demonstrated that TGFβ can promote CSR to IgG2b in LPS-activated B cells and can promote serum antigen-specific IgG2b following mucosal immunization (Borsutzky et al., 2004). However, serum IgG2b was not reduced in unimmunized animals lacking Tgfbr2 in B cells (Cazac and Roes, 2000), and we did not find reduced CSR to IgG2b in *Cr2-cre Tgfbr1*$^{f/f}$ mixed chimeras (Fig. 3 A). In *Aicda*$^{cre/+}$ *Tgfbr1*$^{f/f}$ PP GCBs, we also saw increased IgG2b and decreased CSR to IgG1 compared with controls (Fig. 3 B).

In T cell–sufficient animals, IgA$^+$ plasma cells in the lamina propria of the small intestine are thought to be principally derived from B cells that have undergone CSR to IgA in PPs (Reboldi and Cyster, 2016; Bunker and Bendelac, 2018). Therefore, to determine whether loss of TGFβ signaling in the GC affects plasma cell output from PPs, we assessed IgA$^+$ plasma cell frequency in small intestine lamina propria or IgA production in cecal contents from *Cr2-cre Tgfbr1*$^{f/f}$ or *Aicda*$^{cre/+}$ *Tgfbr*$^{f/f}$ mice. As expected, in *Cr2-cre Tgfbr1*$^{f/f}$ animals, where TGFβ signaling is lost in the SED and GC, IgA$^+$ plasma cells in the lamina propria and cecal IgA were strongly reduced (Fig. 3, C and D; and Fig. S1, A and B). In contrast, in *Aicda*$^{cre/+}$ *Tgfbr*$^{f/f}$ animals, where TGFβ signaling is strongly reduced in the GC but is still detectable in the SED, IgA$^+$ plasma cells and cecal IgA were detected at levels similar to *Aicda*$^{cre/+}$ *Tgfbr*$^{f/+}$ control animals (Fig. 3, E and F; and

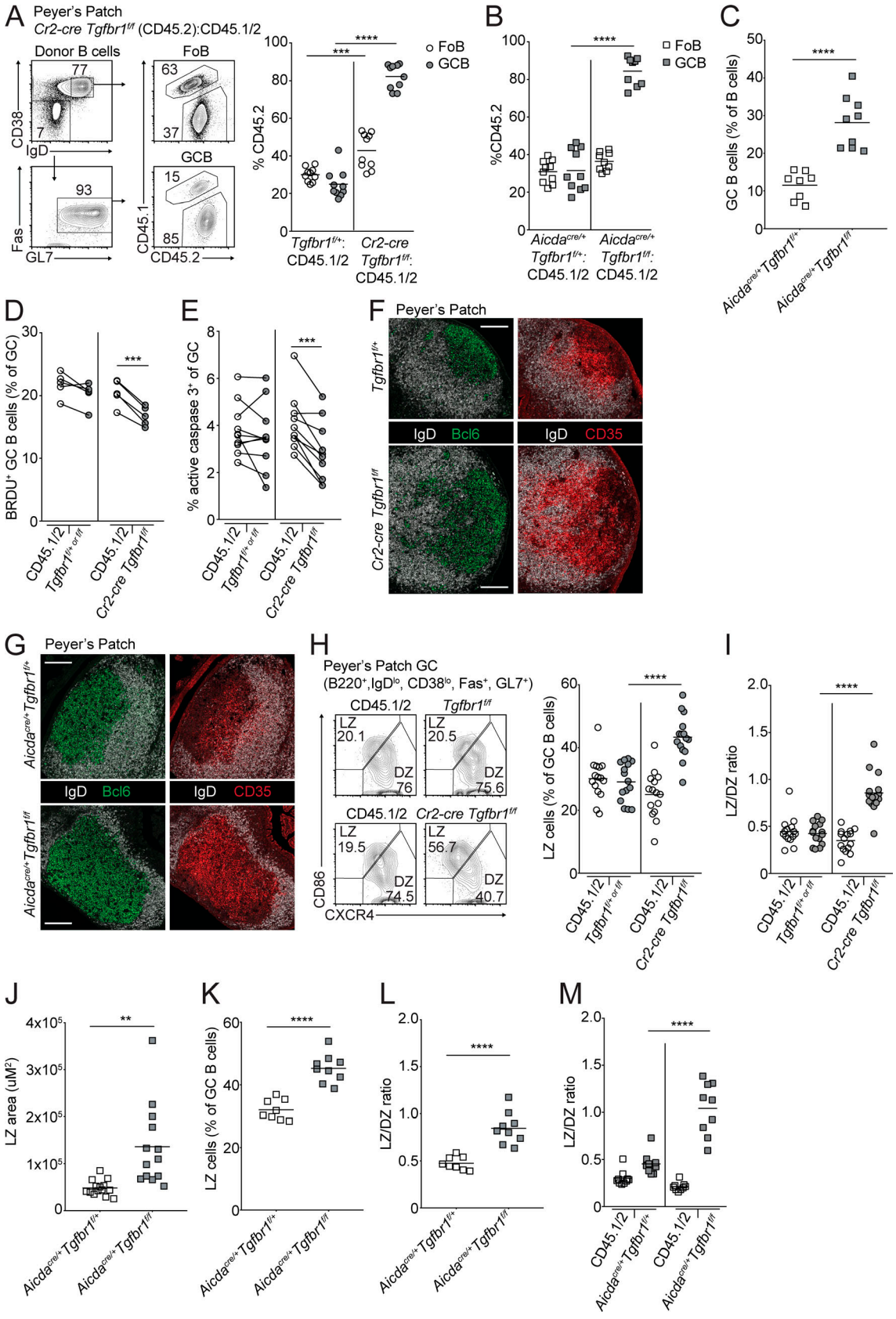

Figure 2. **TGFβ signaling in PP GCs suppresses survival and promotes the transition from the LZ to DZ. (A and B)** Percentages of CD45.2 FoBs and GCBs among cells derived from mixed bone marrow chimeras generated with a mixture of 70% WT (CD45.1/2) and 30% CD45.2 bone marrow that was *Tgfbr1*$^{f/+}$ or *Cr2-cre Tgfbr1*$^{f/f}$ (A) or *Aicda*$^{cre/+}$ *Tgfbr1*$^{f/+}$ or *Aicda*$^{cre/+}$ *Tgfbr1*$^{f/f}$ (B) assessed by FACS. Example gating strategy for FoBs and GCBs is shown on the left in A. Data in

A and B are pooled from two independent experiments with 9–10 total mice in each group. **(C)** Percentage of GCBs among all B cells in PPs of *Aicda*$^{cre/+}$ *Tgfbr1*$^{f/+}$ or *Aicda*$^{cre/+}$ *Tgfbr1*$^{f/f}$ animals. Data are pooled from four independent experiments with eight and nine animals in each group. **(D)** Intracellular FACS for BrdU incorporation in GCBs from PPs of mixed bone marrow chimeras generated as in A that were treated i.p. with BrdU 30 min before sacrifice. Data are from five mice of each type from one experiment representative of two independent experiments. **(E)** Intracellular FACS for active caspase-3 in GCBs from PPs of mixed bone marrow chimeras generated as in A analyzed directly ex vivo. Data are pooled from two independent experiments with a total of nine mice per group. **(F and G)** Confocal microscopy of PPs from *Tgfbr1*$^{f/+}$ or *Cr2-cre Tgfbr1*$^{f/f}$ (F) or *Aicda*$^{cre/+}$ *Tgfbr1*$^{f/+}$ or *Aicda*$^{cre/+}$ *Tgfbr1*$^{f/f}$ (G) animals stained for IgD (white) and Bcl6 (green; left) or CD35 (red; right). Scale bars: 150 µm. Data in F and G are representative of three independent experiments with a total of three to four animals of each type. **(H and I)** Percentage of LZ (H) or ratio of LZ (CD86hiCXCR4lo) to DZ (CD86loCXCR4hi) GCBs (I) from PPs of control or *Cr2-cre Tgfbr1*$^{f/f}$ mixed bone marrow chimeras generated as in A. Representative gating scheme is shown in H. Data in H and I are pooled from three independent experiments with 15 total mice per group. **(J)** Area of LZ in PP GCs from *Aicda*$^{cre/+}$ *Tgfbr1*$^{f/+}$ or *Aicda*$^{cre/+}$ *Tgfbr1*$^{f/f}$ animals as defined by CD35 staining. Data are from 14 and 13 PPs from three mice of each type. **(K and L)** Percentage of LZ cells among all GCBs (K) or ratio of LZ to DZ GCBs (L) in PPs of *Aicda*$^{cre/+}$ *Tgfbr1*$^{f/+}$ or *Aicda*$^{cre/+}$ *Tgfbr1*$^{f/f}$ animals. Data are pooled from four independent experiments with eight and nine animals in each group. **(M)** Ratio of LZ to DZ GCBs from PPs of mixed bone marrow chimeras generated as in B. Data are pooled from two independent experiments with 10 and 9 mice in each group. ***, P < 0.001; paired two-tailed Student's *t* test for data shown in D and E. **, P < 0.01; ***, P < 0.001; ****, P < 0.0001; unpaired two-tailed Student's *t* test for all other data.

Fig. S1, C and D). There was a reduction in cecal IgA in *Aicda*$^{cre/+}$ animals compared with *Aicda*$^{+/+}$ animals, likely as a result of AID heterozygosity (compare control animals in Fig. 3, D and F). These findings suggest that TGFβ signaling within GCBs is not required for CSR to IgA and support a model where CSR to IgA is initiated by TGFβ signaling in the PP SED.

As another test of whether TGFβ signaling in the SED and GC resulted in distinct functional outcomes, we analyzed PP GCBs in Ccr6-deficient mixed bone marrow chimeras. Consistent with published data, in mixed chimeras, IgA was reduced in GCBs derived from Ccr6-deficient bone marrow (Fig. 4 A). However, in contrast to Tgfbr1-deficient mixed chimeras, there was no outgrowth of Ccr6-deficient GCBs (Fig. 4 B); nor was there an increase in LZ GCBs in the absence of Ccr6 in PPs (Fig. 4 C). These data support the hypothesis that TGFβ signaling in B cells in the SED and the GC are functionally distinct.

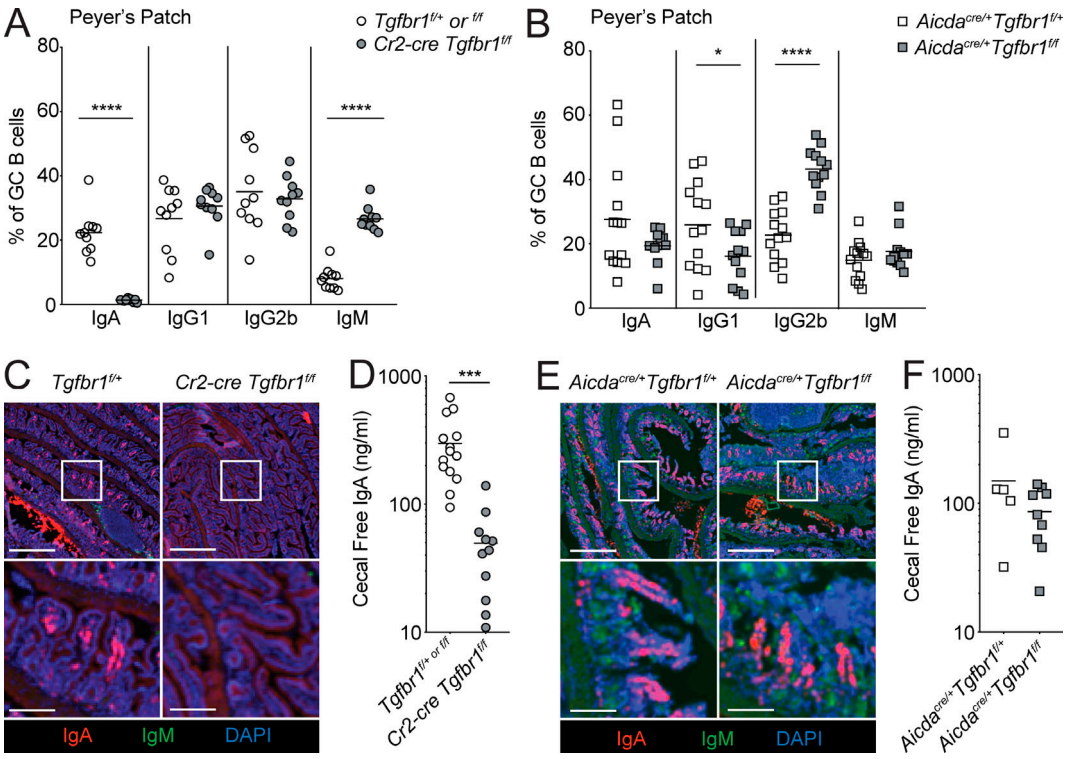

Figure 3. **IgA induction does not require TGFβ signaling in PP GCs. (A and B)** Percentages of CD45.2$^+$ GCBs staining positive for IgA, IgG1, IgG2b, or IgM in PPs from mixed bone marrow chimeras generated with a mixture of 70% WT (CD45.1/2) and 30% CD45.2 bone marrow that was *Tgfbr1*$^{f/+}$ or $^{f/f}$ or *Cr2-cre Tgfbr1*$^{f/f}$ or *Aicda*$^{cre/+}$ *Tgfbr1*$^{f/+}$ or *Aicda*$^{cre/+}$ *Tgfbr1*$^{f/f}$ assessed by FACS. Data in A are pooled from two independent experiments with four to five mice per group. Data in B are pooled from three independent experiments with three to five mice per group. **(C)** Immunofluorescence of sections of small intestine from *Tgfbr1*$^{f/+}$ or *Cr2-cre Tgfbr1*$^{f/f}$ animals stained for IgA (red), IgM (green), and DAPI (blue). Scale bars: 500 µm in low-power images and 125 µm in insets. **(D)** IgA in cecal contents of *Cr2-cre Tgfbr1*$^{f/f}$ animals or littermate controls measured by ELISA. **(E)** Immunofluorescence of sections of small intestine from *Aicda*$^{cre/+}$ *Tgfbr1*$^{f/+}$ or *Aicda*$^{cre/+}$ *Tgfbr1*$^{f/f}$ animals stained as in C. Scale bars: 500 µm in low-power images and 125 µm in insets. **(F)** IgA in cecal contents of *Aicda*$^{cre/+}$ *Tgfbr1*$^{f/+}$ or *Aicda*$^{cre/+}$ *Tgfbr1*$^{f/f}$ measured by ELISA. Data in C and E are representative of three mice of each type from three independent experiments (see Fig. S2 for additional examples). Data in D and F are pooled data from three and two independent experiments, respectively, with 14, 11, 5, and 9 total animals of each type. *, P < 0.05; ***, P < 0.001; ****, P < 0.0001; unpaired two-tailed Student's *t* test.

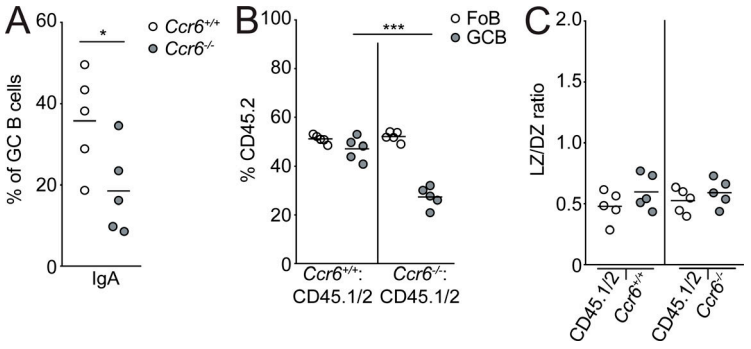

Figure 4. **Ccr6 deficiency does not lead to GC outgrowth or alter GC polarity. (A–C)** Percentages of CD45.2$^+$ GCBs staining positive for IgA (A), frequency of FoBs or GCBs derived from CD45.2 bone marrow (B), or ratio of LZ to DZ GCBs (C) in PPs from mixed bone marrow chimeras generated with a mixture of 50% WT (CD45.1/2) and 50% CD45.2 bone marrow that was *Ccr6*$^{+/+}$ or *Ccr6*$^{-/-}$ assessed by FACS. Data are from five mice of each type from one experiment. *, P < 0.05; ***, P < 0.001; unpaired two-tailed Student's *t* test.

TGFβ signaling promotes the LZ to DZ transition in mLN GCs

Given that GCBs were strongly positive for pSmad2 in PPs, we also examined pSmad2 in GCs in another mucosal lymphoid tissue, the mLN. We found that pSmad2 activity was present in mLN GCs and that staining for pSmad2 was reduced in GCBs in mLNs of *Cr2-cre Tgfbr1*$^{f/f}$ mice (Fig. 5, A and B). In both *Cr2-cre Tgfbr1*$^{f/f}$ and *Aicda*$^{cre/+}$ *Tgfbr1*$^{f/f}$ mixed chimeras, there was an increase in GC representation of Tgfbr1-deficient GCBs in mLNs, although this was significantly lower than what was seen in PPs (compare Fig. 5, C and E to Fig. 2, A and B). There was, however, a similar increase in the proportion of GCBs that were LZ in mLNs compared with PPs in the absence of TGFβ signaling (Fig. 5, D and F). IgA$^+$ GCBs can be found at lower levels in mLNs. In contrast to PPs, we found that there was no reduction in this low level of IgA$^+$ GCBs in mLNs from *Cr2-cre Tgfbr1*$^{f/f}$ mixed chimeras (Fig. 5 G). In mLNs, there is no SED-like structure, and

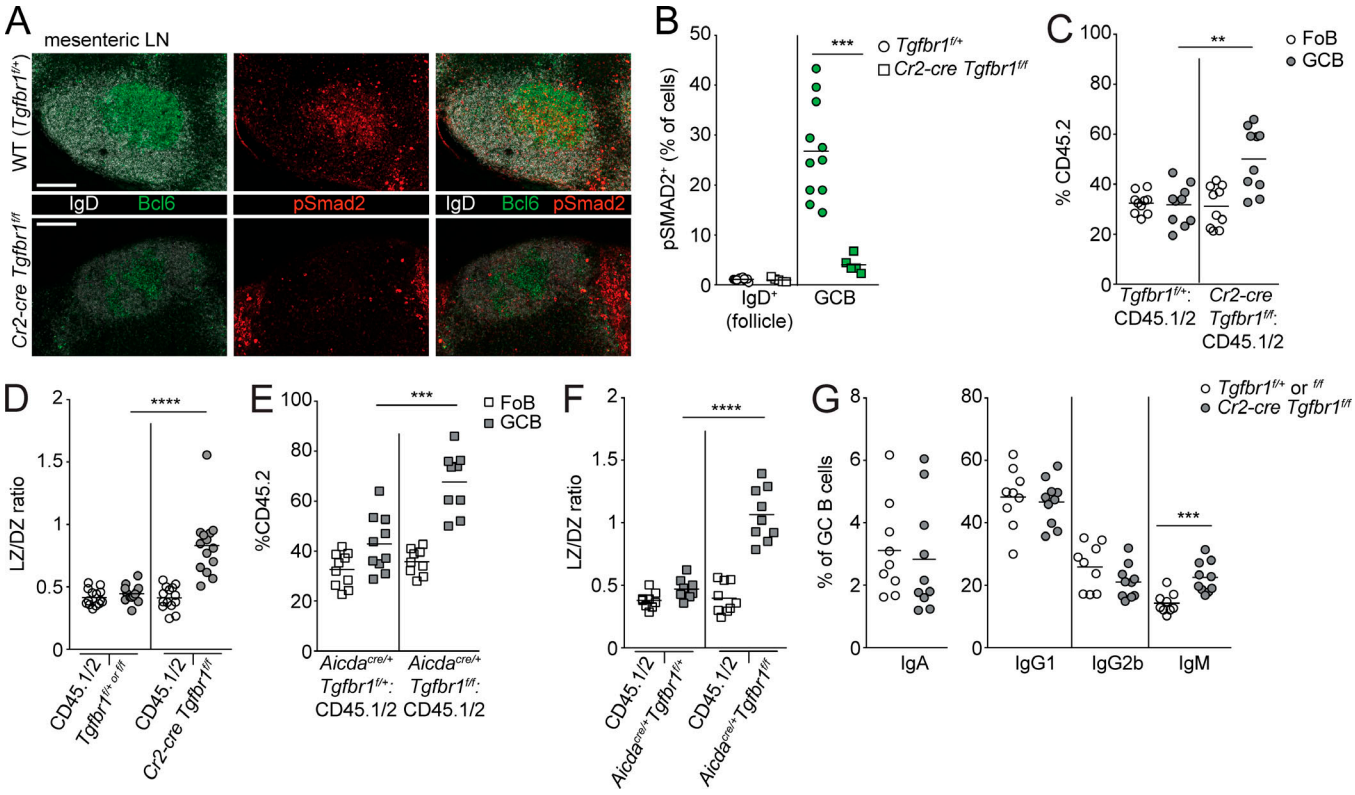

Figure 5. **TGFβ signaling in mLN GCs suppresses survival and promotes the transition from the LZ to DZ. (A)** Confocal microscopy of mLNs of *Tgfbr1*$^{f/+}$ or *Cr2-cre Tgfbr1*$^{f/f}$ animals stained for IgD (white), Bcl6 (green), and pSmad2 (red). Scale bars: 150 µm. **(B)** Percentage of IgD$^+$ B cells in follicle or GC B cells in mLNs staining positive for pSmad2$^+$ quantified by histocytometry. Data in A and B are representative of or are pooled from three experiments with one to three GCs from mLNs from four *Tgfbr1*$^{f/+}$ and three *Cr2-cre Tgfbr1*$^{f/f}$ animals. Each dot represents one GC. **(C and D)** Frequency of FoBs or GCBs derived from CD45.2 bone marrow (C) or ratio of LZ to DZ GCBs (D) in mLNs from mixed bone marrow chimeras generated with a mixture of 70% WT (CD45.1/2) and 30% CD45.2 bone marrow that was *Tgfbr1*$^{f/+}$ or *Tgfbr1*$^{f/f}$ or *Cr2-cre Tgfbr1*$^{f/f}$ assessed by FACS. **(E and F)** Frequency of FoBs or GCBs derived from CD45.2 bone marrow (E) or ratio of LZ to DZ GCBs (F) in mLNs from mixed bone marrow chimeras generated with a mixture of 70% WT (CD45.1/2) and 30% CD45.2 bone marrow that was *Aicda*$^{cre/+}$*Tgfbr1*$^{f/+}$ or *Aicda*$^{cre/+}$ *Tgfbr1*$^{f/f}$ assessed by FACS. **(G)** Percentages of CD45.2$^+$ GCBs staining positive for IgA, IgG1, IgG2b, or IgM from chimeras made as in C. Data in C–G are pooled from two independent experiments with four to five mice per group. **, P < 0.01; ***, P < 0.001; ****, P < 0.0001; unpaired two-tailed Student's *t* test.

IgA induction in mLNs is not dependent on Ccr6 expression in B cells (Reboldi et al., 2016). These data suggest that TGFβ signaling in GCBs in mLNs promotes the transition from LZ to DZ but is not required for CSR to IgA in mLN GCBs.

TGFβ signaling promotes the LZ to DZ transition and antibody affinity maturation in nonmucosal GCs

Given that TGFβ signaling appeared to promote the LZ to DZ transition similarly in GCs in PPs and mLNs, we next asked whether evidence of TGFβ signaling could be detected in GCs in nonmucosal sites. We immunized animals or mixed bone marrow chimeras with sheep RBCs (SRBCs) or the haptenated protein NP-CGG in the adjuvant alum s.c. and examined peripheral LNs (pLNs) 7–10 d after immunization. Similar to other tissues, there was strong pSmad2 activity in pLN GCs, and staining for pSmad2 was greatly reduced in GCBs in pLNs of *Cr2-cre Tgfbr1*$^{f/f}$ mice (Fig. 6, A and B). We next asked whether TGFβ signaling could promote the transition from LZ to DZ in immunized pLNs. By immunofluorescence, in both *Cr2-cre Tgfbr1*$^{f/f}$ and *Aicda*$^{cre/+}$ *Tgfbr1*$^{f/f}$ mice, there was increased LZ on the basis of CD35 staining of FDC (Fig. 6 C and Fig. S2 A). By flow cytometry, the proportion of GCs that were of LZ phenotype was increased in both *Cr2-cre Tgfbr1*$^{f/f}$ and *Aicda*$^{cre/+}$ *Tgfbr1*$^{f/f}$ mixed chimeras (Fig. 6 D and Fig. S2 B). In mixed chimeras, there were no statistically significant changes in CSR to IgA, IgG1, IgG2b, or IgM in the absence of TGFβ signaling (Fig. 6 E and Fig. S2 C). Additionally, in contrast to PPs and mLNs, there was minimal to no growth advantage in Tgfbr1-deficient GCBs in pLNs of immunized mixed chimeras (Fig. 6 F and Fig. S2 D).

Iterative cycling of GCBs between LZ and DZ is thought to be required for optimal antibody affinity maturation (Victora and Nussenzweig, 2012). Given that mature B cell and GCB-specific deletion of Tgfbr1 resulted in an increased fraction of GCBs with an LZ phenotype, we assessed whether Tgfbr1 deficiency affected the generation of high-affinity antibodies against the hapten 4-hydroxy-3-nitrophenylacetyl (NP) 14 d following immunization with NP-CGG in alum. There was a reduced ratio of high-affinity NP-specific IgG1 binding to NP_2 relative to total NP-specific IgG1 binding to NP_{30} in *Cr2-cre Tgfbr1*$^{f/f}$ mice, suggesting a reduction in antibody affinity maturation in the GC (Fig. 6 G). In *Cr2-cre Tgfbr1*$^{f/f}$ mice, we did see a reduction in IgG1 binding to NP_{30} (Fig. S2 E). In *Aicda*$^{cre/+}$ *Tgfbr1*$^{f/f}$ animals, we did not see a reduction of total NP-specific IgG1 binding to NP_{30} but did see a reduction in high-affinity NP-specific IgG1 binding to NP_2, as well as a reduction in the ratio of binding to NP_2 versus NP_{30} compared with *Aicda*$^{cre/+}$ control animals (Fig. 6 H and Fig. S2 F). We next performed repertoire sequencing of the Ig heavy chains of sorted GCBs from *Aicda*$^{cre/+}$ *Tgfbr1*$^{f/+}$ or *Aicda*$^{cre/+}$ *Tgfbr1*$^{f/f}$ animals and analyzed the frequency of NP-specific V_H186.2 IgG1 sequences carrying the high-affinity mutations K59R or Y99G (Furukawa et al., 1999). Because this reaction amplifies heavy-chain RNA from framework region 2 to the constant region, analysis of mutations in CDR1 (such as W33L) was not possible (Yang et al., 2015). We found a reduction in the frequency of sequences carrying the high-affinity mutations K59R or Y99G (Furukawa et al., 1999) in sorted GCBs from *Aicda*$^{cre/+}$ *Tgfbr1*$^{f/f}$ animals compared with *Aidca*$^{cre/+}$ *Tgfbr1*$^{f/+}$ animals (Fig. 6 I and Fig. S2 G). The frequency of total variable region mutations in these sequences was similar in *Aidca*$^{cre/+}$ *Tgfbr1*$^{f/+}$ and *Aicda*$^{cre/+}$ *Tgfbr1*$^{f/f}$ animals (Fig. 6 J and Fig. S2 H). These data suggest that TGFβ signaling in GCBs is required for the generation of high-affinity antibody following immunization with a T-dependent antigen.

TGFβ signaling promotes the transition from the LZ to DZ via Foxo1

The DZ state in the GC is promoted by the nuclear translocation of the transcription factor Foxo1 (Dominguez-Sola et al., 2015; Sander et al., 2015; Inoue et al., 2017). LZ GCBs are known to have increased pAkt relative to DZ. pAkt in LZ cells is thought to phosphorylate Foxo1, prevent its translocation to the nucleus, and target it for degradation (Dominguez-Sola et al., 2015; Sander et al., 2015). In the LZ it has been shown that there is a small fraction of GCBs with active nuclear Foxo1, and it is thought that these are cells that have recently been positively selected by T cells and are transitioning to the DZ. In hematopoietic stem cells, TGFβ signaling has been reported to promote the nuclear translocation of Foxo3, although it is unclear mechanistically how this might occur (Yamazaki et al., 2009; Naka et al., 2010). Recent data in hepatocytes has also shown that TGFβ signaling can induce the dephosphorylation of Foxo1 and promote its activity (Yadav et al., 2017). We hypothesized that one mechanism by which TGFβ signaling might promote the DZ state is via Foxo1. We assessed Foxo1 levels in GCBs from pLNs and PPs of *Cr2-cre Tgfbr1*$^{f/f}$ mixed chimeras via intracellular FACS. We found that Foxo1 protein was reduced in Tgfbr1-deficient GCBs compared with control (Fig. 7 A and Fig. S3 A). LZ cells have less total Foxo1 than DZ cells (Inoue et al., 2017), and so the difference in Foxo1 levels in Tgfbr1-deficient GCBs could have been due to the presence of more LZ GCBs derived from Tgfbr1-deficient bone marrow. However, when we gated on LZ GCBs, we found reduced total Foxo1 in Tgfbr1-deficient LZ cells from both pLNs and PPs compared with control (Fig. 7 B and Fig. S3 B). There was also a reduction in Foxo1 in Tgfbr1-deficient DZ GCBs. We analyzed Foxo1 localization in GCBs from pLNs from *Cr2-cre Tgfbr1*$^{f/f}$ and control mice by immunofluorescence. In control animals, a fraction of LZ GCBs could be found with nuclear Foxo1. Immunofluorescence of pLNs from *Cr2-cre Tgfbr1*$^{f/f}$ animals showed reduced intensity of Foxo1 staining, consistent with data obtained by FACS, and there were fewer cells in the LZ of Tgfbr1-deficient GCs, where Foxo1 was localized in the nucleus (Fig. 7, C and D). The reduction in Foxo1 protein was likely due to a post-translational mechanism, as we did not see a reduction in Foxo1 mRNA in Tgfbr1-deficient GCBs (Fig. 7 E).

In conditions where Akt signaling is increased in GCBs, there is an accumulation of LZ phenotype cells due to increased phosphorylation of Foxo1, which prevents nuclear translocation and promotes its degradation (Sander et al., 2015). Therefore we sought to perturb the Akt/Foxo1 axis in GCBs to determine if this resulted in effects similar to Tgfbr1 deficiency in terms of GC outgrowth and polarity. We assessed the effect of conditional expression of a constitutively active Akt (myristolated Akt; myrAkt) in B cells by reconstituting irradiated hosts with *Cr2-cre*

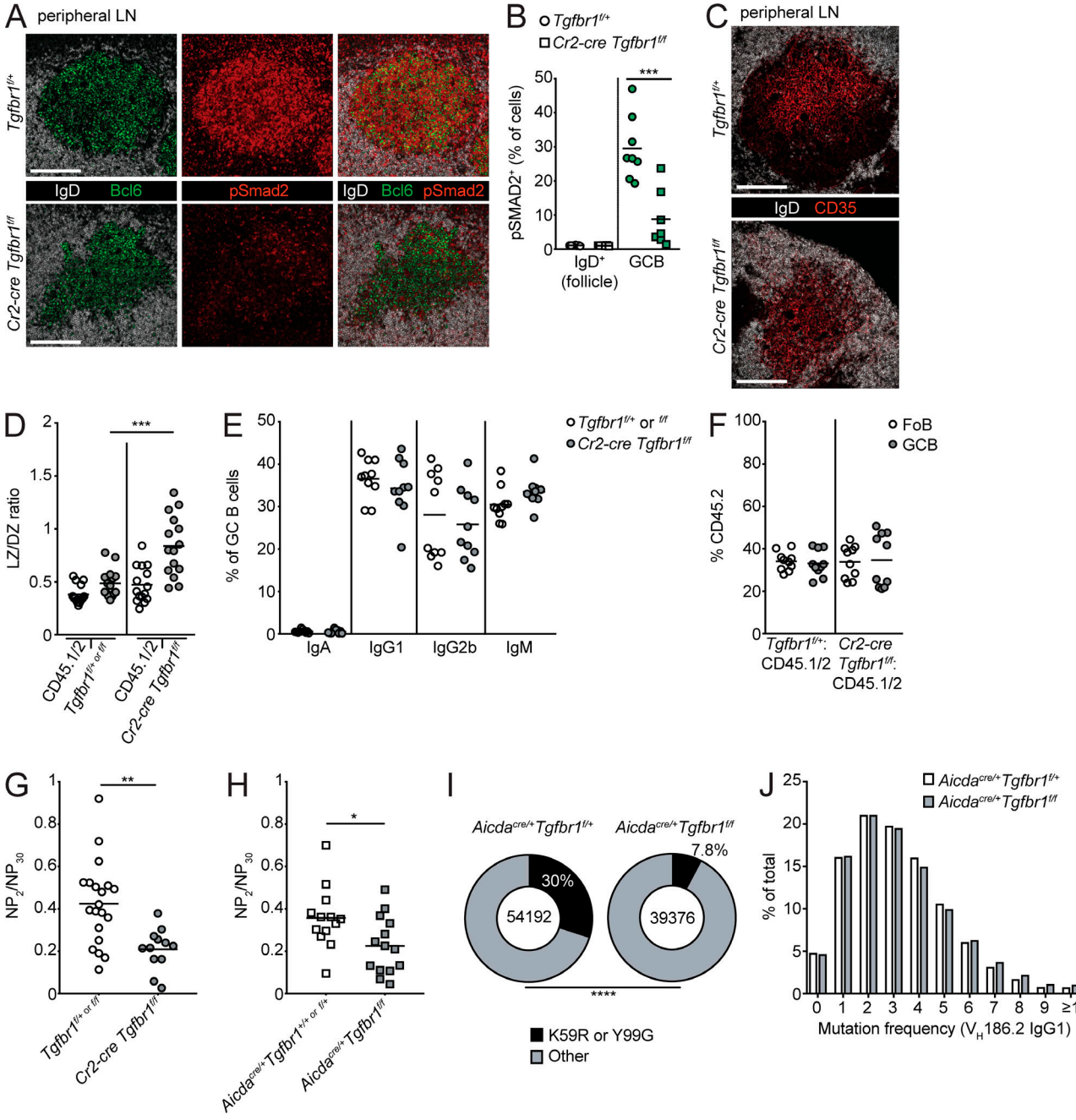

Figure 6. **TGFβ signaling promotes the LZ to DZ transition and antibody affinity maturation in nonmucosal GCs. (A)** Confocal microscopy of pLNs of *Tgfbr1*$^{f/+}$ or *Cr2-cre Tgfbr1*$^{f/f}$ animals that had been immunized s.c. with SRBCs stained for IgD (white), Bcl6 (green), and pSmad2 (red). Scale bar, 150 µm. **(B)** Percentage of IgD$^+$ B cells in follicle or GC B cells in pLNs staining positive for pSmad2 quantified by histocytometry. Data in A and B are representative of or pooled from three to five GCs per mouse from two mice of each type from two independent experiments. Each dot represents one GC. **(C)** Confocal microscopy of pLNs from immunized *Tgfbr1*$^{f/+}$ or *Cr2-cre Tgfbr1*$^{f/f}$ animals stained for IgD (white) and CD35 (red). Scale bars: 150 µm. Data are representative of two independent experiments with a total of four mice per group. **(D–F)** Ratio of LZ to DZ GCBs (D); percentages of CD45.2$^+$ GCBs staining positive for IgA, IgG1, IgG2b, or IgM (E); or frequency of FoBs or GCBs derived from CD45.2 bone marrow (F) in SRBC-immunized pLNs from mixed bone marrow chimeras generated with a mixture of 70% WT (CD45.1/2) and 30% CD45.2 bone marrow that was *Tgfbr1*$^{f/+}$ or $^{f/f}$ or *Cr2-cre Tgfbr1*$^{f/f}$ assessed by FACS. Data in D are pooled from three independent experiments with 15 and 14 total mice in each group. Data in E and F are pooled from two independent experiments with 10 total mice per group. **(G and H)** Ratio of high-affinity IgG1 binding to NP (NP_2) versus total IgG1 binding to NP (NP_{30}) in serum of littermate control or *Cr2-cre Tgfbr1*$^{f/f}$ (G) or *Aicda*$^{cre/+}$ *Tgfbr1*$^{f/+}$ or *Aicda*$^{cre/+}$ *Tgfbr1*$^{f/f}$ (H) animals that had been immunized 14 d prior with NP-CGG in alum by ELISA. Data in G are pooled from two independent experiments with 19 and 12 total mice per group. Data in H are pooled from three independent experiments with 12 and 14 total mice per group. **(I and J)** Frequency of K59R or Y99G mutations (I) or overall variable region mutation frequency (J) in V_H186.2 IgG1 reads from heavy-chain repertoire sequencing (see Materials and methods) of pLN GCBs from NP-CGG–immunized *Aicda*$^{cre/+}$ *Tgfbr1*$^{f/+}$ or *Aicda*$^{cre/+}$ *Tgfbr1*$^{f/f}$ animals. Data are pooled from three mice per group from one experiment. *, P < 0.05; **, P < 0.01; ***, P < 0.001; unpaired two-tailed Student's *t* test for data in A–H. ****, P < 0.0001; χ^2 test for I.

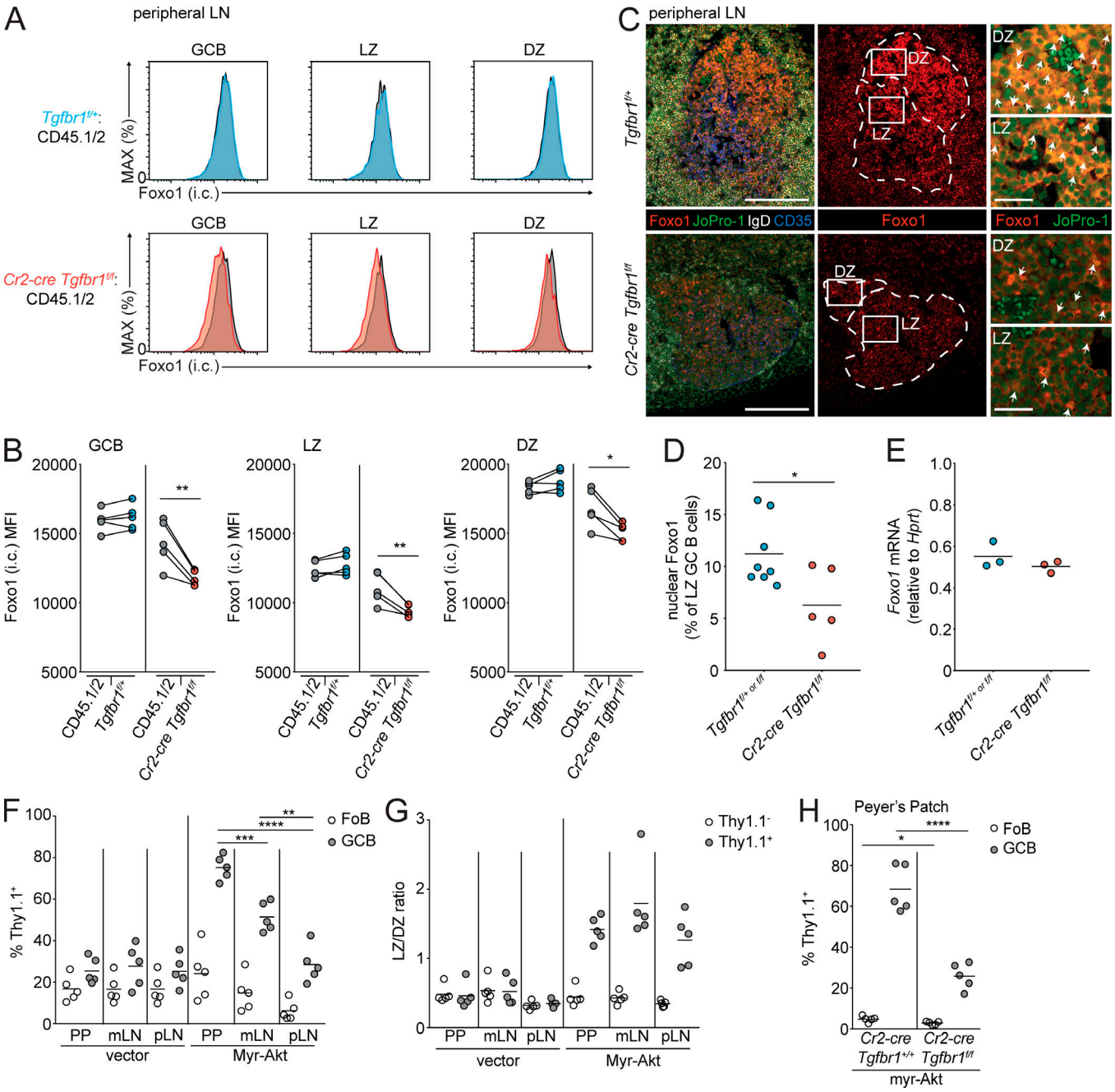

Figure 7. **TGFβ signaling promotes the transition from the LZ to DZ via Foxo1. (A and B)** Intracellular FACS of Foxo1 in total (left), LZ (middle), and DZ (right) GCBs from immunized pLNs of mixed chimeras generated with 30% CD45.2 bone marrow *Tgfbr1*$^{f/+}$ (blue) or *Cr2-cre Tgfbr1*$^{f/f}$ (red) and 70% WT CD45.1/2 (gray) bone marrow. Representative histograms are shown in A, and mean fluorescence intensity (MFI) is shown in B. Data are from five mice of each type from one experiment representative of two independent experiments. MAX, maximum. **(C)** Immunofluorescence of SRBC-immunized pLNs of *Tgfbr1*$^{f/+}$ or *Cr2-cre Tgfbr1*$^{f/f}$ animals stained for Foxo1 (red), the nuclear stain JoPro-1 (green), IgD (white), and CD35 (blue). Scale bars: 150 µm in images of total GC and 25 µm in enlarged sections of LZ and DZ. **(D)** Quantification of the frequency of LZ GCBs with nuclear Foxo1 staining in immunized pLNs of control or *Cr2-cre Tgfbr1*$^{f/f}$ animals. Data in C and D are representative of or pooled from three control and two *Cr2-cre Tgfbr1*$^{f/f}$ mice from two independent experiments. Each dot represents one GC. **(E)** Quantitative PCR of *Foxo1* in sorted GCBs from immunized pLNs of littermate control or *Cr2-cre Tgfbr1*$^{f/f}$ animals. Data in E are from three mice of each type from one experiment representative of two independent experiments. **(F)** Transduced (Thy1.1$^+$) cell frequency among FoBs or GCBs in PPs, mLNs, and SRBC-immunized pLNs of bone marrow chimeras generated with *Cr2-cre* bone marrow transduced with conditional retrovirus expressing consitutively active Akt (myrAkt) or control retrovirus (vector). **(G)** LZ to DZ ratio of untransduced (Thy1.1$^-$) or transduced (Thy1.1$^+$) GCBs from bone marrow chimeras generated as in F. **(H)** Transduced (Thy1.1$^+$) cell frequency among FoBs or GCBs in PPs of bone marrow chimeras generated with *Cr2-cre Tgfbr1*$^{+/+}$ or *Cr2-cre Tgfbr1*$^{f/f}$ bone marrow transduced with conditional retrovirus expressing myrAkt. Data in F and G are from five mice per group from one experiment representative of two independent experiments. Data in H are from five mice per group from one experiment. *, P < 0.05; **, P < 0.01; paired two-tailed Student's *t* test for data in B. *, P < 0.05; **, P < 0.01; ***, P < 0.001; ****, P < 0.0001; unpaired two-tailed Student's *t* test for all other data.

BM transduced with retrovirus expressing myrAkt or human CD4 downstream of a lox stop lox cassette followed by internal ribosomal entry sequence and the reporter Thy1.1 (Green et al., 2011). We found that similar to Tgfbr1 deficiency, myrAkt induced GC outgrowths most strongly in PPs, to an intermediate extent in mLNs, and to a lesser extent in immunized pLNs (Fig. 7 F). MyrAkt was able to increase LZ phenotype to a similar extent in GCs from all tissues analyzed, which was also very similar to the effects of Tgfbr1 deficiency (Fig. 7 G). If TGFβ is perturbing the Akt/Foxo1 axis in vivo, we hypothesized that overexpression of myrAkt in Tgfbr1-deficient GCBs would be less able to drive outgrowths in PP GCs. We tested this by reconstituting irradiated hosts with *Cr2-cre Tgfbr1*$^{f/f}$ or *Cr2-cre Tgfbr1*$^{+/+}$ BM transduced with retrovirus conditionally expressing myrAkt and the reporter Thy1.1. In the Tgfbr1-sufficient setting, myrAkt was able to strongly promote the outgrowth of PP GCs. However, in the absence of Tgfbr1, myrAkt-induced outgrowth of PP GCBs was reduced, suggesting that loss of Tgfbr1 acts in the same pathway as constitutively active Akt to drive GC outgrowth in the PPs (Fig. 7 H). These data suggest that one mechanism by which TGFβ signaling promotes the transition from LZ to DZ is via activation of Foxo1 and that in the absence of TGFβ signaling, there is likely a perturbation of the Akt/Foxo1 axis in GCBs.

FDCs promote TGFβ signaling in the GC

In the SED of PPs, DCs activate latent TGFβ via the expression of the integrin pair αv-β8 and present active TGFβ to activated IgD$^+$ pre-GCBs to promote induction of IgA (Reboldi et al., 2016). In the GC, it has been proposed that FDCs from mucosal tissues also express integrins and other molecules that can promote the activation of TGFβ (Suzuki et al., 2010). Recent single-cell analysis of pLN stromal cell populations has also shown that FDCs express integrin αv more highly than other stromal populations (Rodda et al., 2018). To test whether FDCs could promote TGFβ signaling in GCs, we irradiated Cr2-cre animals that also expressed the diphtheria toxin (DTx) receptor (DTR) downstream of a loxp-stop-loxp cassette in the Rosa26 locus (Cr2-DTR mice; Wang et al., 2011) and reconstituted them with EμBcl2 bone marrow in which Bcl2 is overexpressed by all B cells (EμBcl2 Cr2-DTR; Strasser et al., 1991). In these animals, DTR is expressed on Cr2-expressing nonhematopoietic cells, which include FDCs and other stromal cell types that express lower levels of Cr2 and can be ablated following administration of DTx (Wang et al., 2011; Jarjour et al., 2014). We used EμBcl2 bone marrow so that GC structures in mucosal tissues would persist even after loss of pro-survival cues provided by FDCs to GCBs (Wang et al., 2011). 1 d after DTx administration, CD35 staining was significantly reduced in EμBcl2 Cr2-DTR mice compared with controls (Fig. 8 A). We found that pSmad2 activity in GCs was significantly reduced following FDC ablation (Fig. 8, B and C). It is possible that FDCs are promoting the ability of another cell type to activate and present TGFβ to GCBs. Other cell types that could promote activation of TGFβ in the GC are T follicular helper cells or T follicular regulatory cells. Therefore, we depleted CD4$^+$ T cells for 1 d and assessed pSmad2 activity before GC collapse (Fig. 8 D). We found that acute depletion of CD4$^+$ T cells did not reduce pSmad2 in PP GCs, suggesting that T follicular helper cells or T follicular regulatory cells are not the primary source of active TGFβ for GCBs (Fig. 8, E and F). These data show that Cr2-expressing stromal cells such as FDCs are required to promote TGFβ signaling in GCBs.

Discussion

In this study, we showed that TGFβ signaling in GCBs is critical for GC homeostasis and function in mucosal and nonmucosal lymphoid tissue. We showed that TGFβ signaling within GCBs is distinct from signaling that occurs in the SED of PPs and that TGFβ signaling in the GC is dispensable for IgA induction. We showed that TGFβ signaling in GCBs is important for promoting the transition from LZ to DZ in all GCs and for supporting antibody affinity maturation, possibly via activation of the transcription factor Foxo1. Finally, we demonstrated that FDCs are likely critical for promoting TGFβ signaling in GCBs.

The original study identifying the critical role of TGFβ signaling in IgA induction reported GC hyperplasia in animals lacking Tgfbr2 in B cells (Cazac and Roes, 2000). Additionally, in conditions with excess TGFβ receptor in B cells, there is a reduced contribution to PP GCs (Wu et al., 2016). However, GC outgrowths have not been reported when B cells lack Ccr6, despite a decrease in IgA (Reboldi et al., 2016). Our study resolves this discrepancy by showing that there are distinct sites of TGFβ signaling within the PPs and that TGFβ signaling in these sites is associated with distinct functional outcomes. Specifically, our data show that when there is loss of TGFβ signaling primarily in GCBs, as in *Aicda*$^{cre/+}$ *Tgfbr1*$^{f/f}$ mice, induction of IgA can still occur, but loss of TGFβ signaling in the GC leads to an accumulation of LZ cells in the PPs. However, when activated pre-GCBs have reduced access to the SED and decreased TGFβ signaling in that location, as in Ccr6 deficiency, TGFβ signaling can still occur in the GC, but there is reduced IgA and no outgrowth or LZ bias of PP GCBs.

Several recent studies have highlighted the importance of the transcription factor Foxo1 in sustaining the DZ state and promoting affinity maturation in the GC (Dominguez-Sola et al., 2015; Sander et al., 2015; Inoue et al., 2017). These studies also demonstrated increased activity of pAkt in LZ GCBs and proposed that Akt signaling sustains the LZ state by phosphorylating Foxo1 and targeting it for degradation. However, whether there are signals in the GC microenvironment that promote activation of Foxo1 to allow for LZ cells to transition to the DZ state has not previously been demonstrated. Our data support the hypothesis that TGFβ signaling in LZ GCBs promotes the transition to the DZ state via nuclear translocation of Foxo1. In the absence of TGFβ signaling, Foxo1 mRNA is not significantly reduced, suggesting that Foxo1 is regulated by TGFβ signaling via a nontranscriptional mechanism. Upon ligation, TGFβ receptor has been reported to interact with and promote the activity of protein phosphatase 2a (PP2A), and in hepatocytes, TGFβ-mediated activation of PP2A has been reported to dephosphorylate Foxo1 and promote its activity (Petritsch et al., 2000; Yadav et al., 2017). Whether TGFβ-mediated activation of PP2A or a similar mechanism occurs in GCBs to activate Foxo1 and promote the LZ to DZ transition warrants further study.

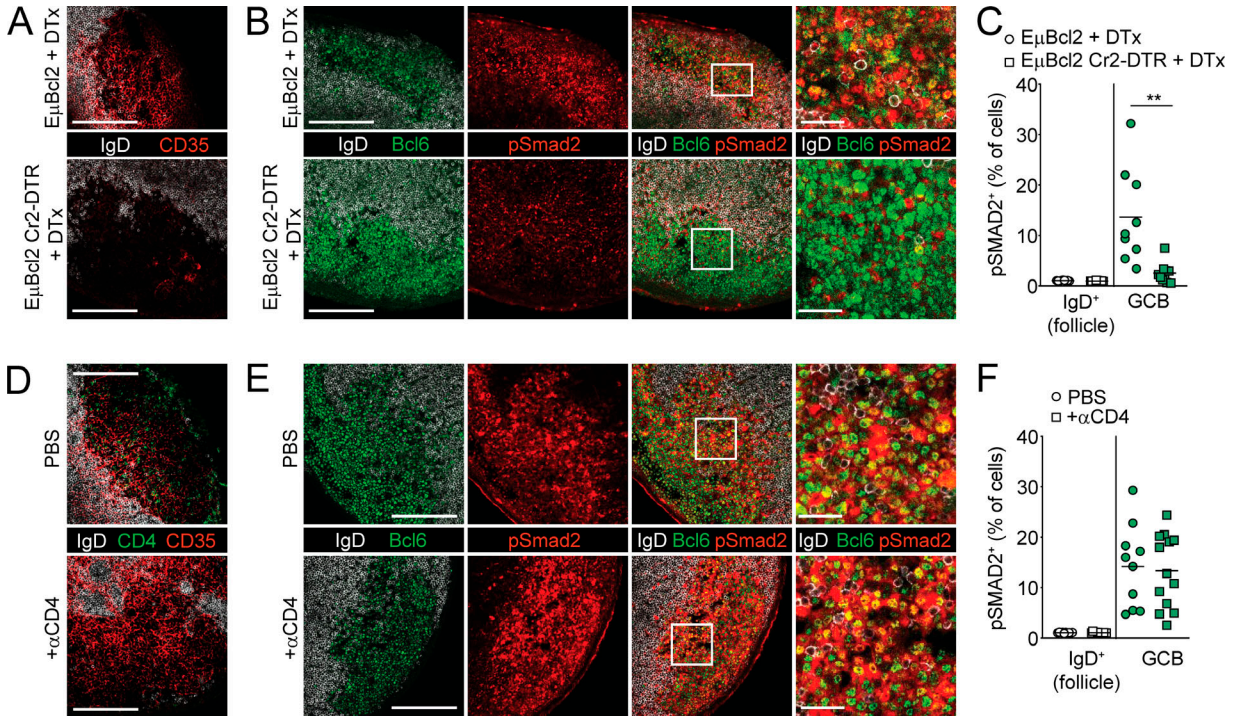

Figure 8. **FDCs promote TGFβ signaling in GCBs. (A–C)** Immunofluorescence of PPs from lethally irradiated Cr2-DTR or control animals that were reconstituted with EμBCL2 bone marrow and were treated with DTx 18 h before sacrifice and stained with IgD, Bcl6, and CD35 (A) or IgD, Bcl6, and pSmad2 (B). Histocytometric analysis of pSmad2 staining is shown in C. Data in A and B are representative of and C is pooled from three and four mice per group with one to three PP GCs analyzed per mouse from two independent experiments. Each dot represents one GC. **(D–F)** Immunofluorescence of PPs from WT animals that were treated 1 d previously with PBS or 200 µg anti-CD4 depleting antibody and stained for IgD, CD35, and CD4 (D) or IgD, Bcl6, and pSmad2 (E). Histocytometric analysis of pSmad2 staining is shown in F. Data in D and E are representative of and in F is pooled from three mice per group with three to five PP GCs analyzed per mouse from two independent experiments. Each dot represents one PP. Scale bars: 150 µm in images of total GC and 25 µm in enlarged sections of GC. **, $P < 0.01$; unpaired two-tailed Student's *t* test.

It is currently unclear why loss of TGFβ signaling or increased activation of Akt promotes survival of GCBs more strongly in mucosal tissues such as PPs than nonmucosal sites despite evidence of active signaling in both sites and similar perturbations in GC polarity in all sites. We are currently trying to identify factors in the GC microenvironment in PPs and mLNs that might cooperate with loss of TGFβ signaling or increased Akt to promote greater GCB survival in mucosal lymphoid tissues compared with nonmucosal lymphoid tissues.

Our data support a model where FDCs activate TGFβ in the GC to promote TGFβ signaling in GCBs. However, we cannot exclude the possibility that FDCs might indirectly promote TGFβ signaling via another cell type. Future studies are needed to address whether expression of TGFβ-activating integrins in FDCs or another cell type is required for TGFβ signaling in GCBs.

In summary, our study provides evidence that TGFβ signaling occurs at two distinct stages of B cell differentiation and that signaling in activated IgD$^+$ B cells in the PP SED and in GCBs is associated with distinct functional outcomes. We identified TGFβ signaling in GCBs as an important microenvironmental cue that promotes the transition from LZ to DZ, possibly via Foxo1, and supports antibody affinity maturation. Defining microenvironmental cues in the GC that regulate GC homeostasis, polarity, and function is critical to understanding the humoral immune response.

Materials and methods

Animals and treatments

Adult C57BL6 CD45.1$^+$ (stock number 564) and C57BL/6NCr (stock number 556) mice ≥7 wk of age were from Charles River Frederick Research Model Facility. *Cr2-cre* (B6.Cg-Tg[Cr2-cre]3Cgn/J; stock number 006368), *Aicda$^{cre/cre}$* (B6.129P2-*Aicda$^{tm1(cre)Mnz}$*/J; stock number 007770), *Ccr6$^{-/-}$* (B6.129P2-*Ccr6^{tm1Dgen}*/J; stock number 005793), and ROSA-DTR (C57BL/6-*Gt(ROSA)26Sor$^{tm1(HBEGF)Awai}$*; stock number 007900) mice were on a B6 background and were from The Jackson Laboratory. *Tgfbr1$^{f/f}$* mice were on a B6 background (provided by Wanjun Chen, National Institute of Dental and Craniofacial Research, National Institutes of Health, Bethesda, MD). EμBcl2 mice overexpress *BCL2* selectively in B cells (Strasser et al., 1991). Bone marrow chimeras were made using CD45.1$^+$ from Charles River or Cr2-DTR mice as hosts. Hosts were lethally irradiated with 900 rad in split doses and reconstituted with at least 3×10^6 BM cells from the indicated donors. Mice were analyzed ≥7 wk after reconstitution. For FDC ablation, Cr2-DTR reverse chimeras were treated with a single dose of 100 ng of DTx (EMB Biosciences) 18 h before sacrifice. For CD4 depletion, WT B6 animals were treated with 200 µg of anti-CD4 (GK1.5; BioXcell) 1 d before sacrifice. Mice were housed in a specific pathogen–free environment, and all mouse experiments were approved by the National Cancer Institute Animal Care and Use Committee and were performed in accordance with the Committee's guidelines and under approved protocols.

Immunofluorescence and histocytometry

Tissues were fixed in BD Cytofix/Cytoperm diluted 1 to 4 in PBS overnight at 4°C, washed three times in PBS, then moved to 30% sucrose in PBS overnight. Tissues were flash-frozen in optimal cutting temperature compound (Sakura) the following day. 30-µm sections were cut on a Leica CM3050S cryostat and were adhered to Super Frost Plus slides (Fisher Scientific) and then stored at −80°C. Prior to staining, sections were permeabilized in ice-cold methanol for 30–60 min. When necessary, endogenous peroxidase activity was blocked by incubating tissue for 1 h at 27°C with 3% H_2O_2 (Tyramide SuperBoost Kit; Invitrogen). Sections were blocked for 1 h in PBS containing 0.3% Triton X-100, 1% BSA, 2% normal mouse serum, 2% normal goat serum, 2% normal rat serum, and 2% anti-CD16/32 (BioXcell). Sections were stained with Alexa Fluor (AF) 700–conjugated anti-B220 (RA3-6B2; BioLegend); AF488-, AF647-, or AF594-conjugated anti-IgD (11-26c.2a; BioLegend); AF647-conjugated anti-BCL6 (K112-91; BD); AF488-conjugated anti-CD11c (N418; BioLegend); FITC-conjugated anti-CD11c (7E9; BioLegend); BV421-conjugated anti-CD4 (RM4-5; BioLegend); biotin-conjugated anti-CD35 (8C12; BD); rabbit anti-pSmad2 (S465/467; 138D4; Cell Signaling); and/or rabbit anti-Foxo1 (C29H4; Cell Signaling) overnight at 4°C in a humidified chamber. Secondary antibodies were BV421-conjugated streptavidin (BioLegend), AF488-conjugated anti-FITC (Jackson Immunoresearch), AF555-conjugated streptavidin (Invitrogen), and/or AF555-conjugated anti-rabbit IgG (Invitrogen) and were incubated with slides for 3 h at 27°C. For detection of pSmad2 and Foxo1, the primary antibody was labeled with HRP-conjugated anti-rabbit, and the signal was amplified with an AF555-conjugated Tyramide SuperBoost Kit (7 min for pSmad2 and 10 min for Foxo1; Invitrogen) according to the manufacturer's instructions. Cell nuclei were stained with JoPro-1 (Fisher Scientific). Stained slides were mounted with Fluoromount G (eBioscience) and sealed with a glass coverslip. Tile scans of PPs were acquired using an SP8 confocal microscope (Leica Microsystems) with 40× or 63× oil immersion objective NA1.3. For histocytometric analysis of pSmad2 intensity in SED and GCBs, we stained PP sections with a panel consisting of the following fluorophores: AF488, JoPro-1, AF555, AF594, AF647, and AF700. Fluorophore emission was collected on separate detectors with sequential laser excitation. Channel dye separation was accomplished using LAS X software (Leica Microsystems). Three-dimensional image reconstruction and surface rendering was performed as previously described (Gerner et al., 2012; Radtke et al., 2015). Representative tile scans were taken at a voxel density of 512 × 512 and a 5-µm z step. Channel statistics for all surfaces were exported into Excel (Microsoft) and converted to a CSV file for direct visualization in FlowJo. Single cells were identified on the basis of $B220^+$, IgD^+, $BCL6^+$, and $CD11c^+$ to identify FoBs ($B220^+$ IgD^+), GCBs ($B220^+$ IgD^- $BCL6^+$), and DCs ($CD11c^+$). SED and GC gates were defined using positional data on $CD11c^+$ and IgD^- $BCL6^+$ surfaces, respectively. These positional gates were then applied to the $B220^+$ surfaces to calculate the frequency of $pSmad2^+$ IgD^+ events in the SED or $pSmad2^+$ IgD^- $BCL6^+$ events in the GC. For assessment of the frequency of LZ cells with nuclear Foxo1, CD35 was used to determine LZ location, and LZ cells with co-localized Foxo1/JoPro-1 were counted and divided by total number of cells in the LZ. The frequency of LZ cells with nuclear Foxo1 was also independently assessed by a blinded observer. For imaging of small intestine, samples were fixed, dehydrated, and frozen as above, and 7-µm sections were cut and fixed in cold acetone for 10 min. Sections were stained with biotinylated anti-IgA (RMA-1; BioLegend), FITC-conjugated anti-IgM (BioLegend) followed by streptavidin conjugated to AF55 (Life Technologies), AF488-conjugated anti-FITC (Jackson Immunoresearch), and DAPI. Images were acquired on a Zeiss AxioObserver Z1.

Flow cytometry

PP, mLN, and pLN cell suspensions were generated by mashing the organs through 70-mm cell strainers in RPMI containing 2% (vol/vol) FBS, antibiotics (penicillin [50 IU/ml] and streptomycin [50 mg/ml]; Cellgro), and 10 mM Hepes, pH 7.2 (Cellgro). Flow cytometry was performed on a Cytoflex LX (Beckman Coulter). For GCB analysis, cells were stained with BUV395-conjugated anti-B220 (RA3-6B2; BD), BV605-conjugated anti-CD4 (RM4-5; BioLegend), Pacific blue–conjugated anti-GL7 (GL7; BioLegend), BV650-conjugated anti-IgD (11-26c.2a; BioLegend), PE-Cy7–conjugated anti-CD38 (90; BioLegend), PE-Cy7- or PE-conjugated anti-Fas (Jo2; BD), FITC-conjugated anti-CD45.2 (104; BioLegend), PerCP-Cy5.5–conjugated anti-CD45.1 (A20; BioLegend), BV786-conjugated anti-CD86 (GL-1; BioLegend), biotinylated anti-CXCR4 (2B11; eBioscience), BV605 conjugated to streptavidin (BD), PE-conjugated goat anti-mouse IgA (Southern Biotech), APC-conjugated anti-IgG1 (RMG1-1; BioLegend), PE-conjugated anti-IgG2b (RMG2b-1; BioLegend), and/or APC-conjugated anti-IgM (II/41; BD). For BrdU incorporation experiments, animals were given 2.5 mg BrdU in a single i.p. injection and sacrificed 30 min later, and staining was performed using the FITC BrdU Flow Kit (BD PharMingen). For anti–active caspase-3 staining, cells were maintained on ice during harvesting and processing to minimize cell death ex vivo, and cells were stained for surface markers, fixed and permeabilized using the BD cytofix/cytoperm kit, and stained with active caspase-3 (C92-605; BD) according to the manufacturer's instructions. For intracellular staining of total Foxo1, cells were stained for surface markers and fixed and permeabilized using True-Nuclear Transcription Factor Buffer Set (BioLegend) and stained with anti-Foxo1 (C29H4; Cell Signaling) followed by AF647-conjugated goat anti-rabbit IgG (Life Technologies) according to the manufacturer's instructions.

Immunizations and ELISAs

For serum antibody responses, mice were immunized s.c. with a total of 100 µg NP-CGG (Biosearch Technologies Inc.) in alum (Sigma-Aldrich) divided among four sites. Serum was prepared from blood collected from the retro-orbital space 14 d later. For detection of cecal IgA, cecal matter was suspended in PBS at 50 mg/ml and centrifuged at 400 *g* for 5 min, supernatant was collected and centrifuged again at 8,000 *g* for 10 min, and supernatants were used for detection. Microtiter plates were coated overnight at 4°C with 10 µg/ml NP_2 or NP_{30}-BSA (Biosearch Technologies Inc.) or 2 µg/ml anti-IgA (C10-3; BD) diluted in carbonate buffer, pH 9.6. Washing was with PBS with 0.1% Tween-20 (PBST), blocking was with PBST/5% BSA, and serum or cecal supernatants were diluted in PBST/1% BSA. Serum or cecal dilutions were incubated in the coated wells for 1 h, and bound antibodies were detected using anti-IgG1 or anti-IgA conjugated to HRP (Southern Biotech) developed with 3,3′,5,5′

tetramethyl benzidine (BioLegend). Reactions were stopped after 5 min with 2 N H_2SO_4. Absorbance was measured at 450 nm in a SpectraMax M3 microplate reader using SoftMax pro 7.0 (Molecular Devices). Purified mouse IgA (Southern Biotech) served as the standard for cecal samples.

RNA isolation, RT-PCR, and assessment of high-affinity mutations in Vh186.2

GCBs from pLNs were sorted directly into TRIzol LS reagent (Life Technologies), and RNA was extracted according to the manufacturer's protocol. Real-time PCR was performed with SYBR Green PCR Mix (Roche) and an ABI prism 7500 sequence detection system (Applied Biosystems). The following primers were used: *Foxo1* forward, 5′-AGATCTACGAGTGGATGGTGA AGAG-3′; *Foxo1* reverse, 5′-GGACAGATTGTGGCGAATTGAAT-3′; *Hprt* forward, 5′-AGGTTGCAAGCTTGCTGGT-3′; *Hprt* reverse, 5′-TGAAGTACTCATTATAGTCAAGGGCA-3′. For assessment of K59R or Y99G mutation frequency in Vh186.2 (Ighv72-1*01) IgG1 heavy chains, RNA from 60,000 to 100,000 sorted GCBs was sent on dry ice to iRepertoire, Inc. cDNA synthesis, PCR amplification of heavy-chain repertoire, and analysis on an Illumina MiSeq were performed with proprietary reagents by iRepertoire, Inc (Yang et al., 2015). Approximately 800,000 total reads were obtained for each sample. Because this reaction amplifies heavy-chain RNA from framework region 2 to the constant region, analysis of mutations in CDR1 (such as W33L) was not possible. K59R or Y99G and overall mutation frequency were assessed using IMGT/HighV-Quest and were counted in nonframe-shifted Ighv1-72*01 (Vh186.2) sequences that were also IgG1. K59R or Y99G and overall mutation frequency were assessed in both total Ighv1-72*01 IgG1 reads and in unique sequences that were present in two or more reads.

Bone marrow transduction

For transduction of bone marrow, *Cr2-cre Tgfbr1*$^{+/+}$ or *Cr2-cre Tgfbr1*$^{f/f}$ donor mice were injected intravenously with 3 mg 5-fluorouracil (Sigma-Aldrich). Bone marrow was collected after 4 d and cultured in DMEM containing 15% (vol/vol) FBS, antibiotics (penicillin [50 IU/ml] and streptomycin [50 mg/ml]; Cellgro), and 10 mM Hepes, pH 7.2 (Cellgro), supplemented with IL-3, IL-6, and stem cell factor (at concentrations of 20, 50, or 100 ng/ml, respectively; Peprotech). Cells were "spin infected" twice with retrovirus in which myrAkt or human CD4 (control) was downstream of a loxP–stop–loxP cassette at days 1 and 2 and transferred into irradiated recipients on day 3.

Statistical analysis

Prism software (GraphPad) was used for all statistical analysis. Data were analyzed with a two-sample unpaired (or paired, where indicated) Student's *t* test or χ^2 test. P values were considered significant when ≤ 0.05.

Online supplemental material

Fig. S1 shows additional examples of immunofluorescence of IgA$^+$ cells in small intestine. Fig. S2 shows analysis of the GC response of *Aicda*$^{cre/+}$ *Tgfbr1*$^{f/f}$ in pLNs following immunization. Fig. S3 shows intracellular Foxo1 staining of PP GCBs from mixed chimeras.

Acknowledgments

We thank Wanjun Chen for providing *Tgfbr1*$^{f/f}$ mice, A. Radtke and R. Germain for advice on histocytometry, Michael Kruhlak and Jan Wisniewski for advice and assistance with microscopy and image analysis, S. Carrasco for assistance with image analysis, and O. Bannard, J. Cyster, M. Mintz, L. Rodda, P. Schwartzberg, and C. Wu for helpful discussions and providing comments on the manuscript. Cell sorting was performed in the Center for Cancer Research Flow Cytometry Core Facility.

This research was supported by the Intramural Research Program of the National Institutes of Health, Center for Cancer Research, National Cancer Institute.

The authors declare no competing financial interests.

Author contributions: A.R. Albright designed and performed experiments, analyzed and interpreted data, and edited the manuscript. J. Kabat assisted with the design of microscopy experiments and image analysis. M. Li and F. Raso performed experiments. A. Reboldi designed experiments and edited the manuscript. J.R. Muppidi designed and performed experiments, analyzed and interpreted data, and wrote the manuscript.

Submitted: 1 October 2018
Revised: 18 June 2019
Accepted: 1 August 2019

References

Bannard, O., R.M. Horton, C.D. Allen, J. An, T. Nagasawa, and J.G. Cyster. 2013. Germinal center centroblasts transition to a centrocyte phenotype according to a timed program and depend on the dark zone for effective selection. *Immunity*. 39:912–924. https://doi.org/10.1016/j.immuni.2013.08.038

Borsutzky, S., B.B. Cazac, J. Roes, and C.A. Guzmán. 2004. TGF-β receptor signaling is critical for mucosal IgA responses. *J. Immunol.* 173: 3305–3309. https://doi.org/10.4049/jimmunol.173.5.3305

Bunker, J.J., and A. Bendelac. 2018. IgA responses to microbiota. *Immunity*. 49: 211–224. https://doi.org/10.1016/j.immuni.2018.08.011

Cazac, B.B., and J. Roes. 2000. TGF-β receptor controls B cell responsiveness and induction of IgA in vivo. *Immunity*. 13:443–451. https://doi.org/10.1016/S1074-7613(00)00044-3

Cyster, J.G. 2015. Germinal centers: Gaining strength from the dark side. *Immunity*. 43:1026–1028. https://doi.org/10.1016/j.immuni.2015.11.019

David, C.J., and J. Massagué. 2018. Contextual determinants of TGFβ action in development, immunity and cancer. *Nat. Rev. Mol. Cell Biol.* 19:419–435. https://doi.org/10.1038/s41580-018-0007-0

Dominguez-Sola, D., J. Kung, A.B. Holmes, V.A. Wells, T. Mo, K. Basso, and R. Dalla-Favera. 2015. The FOXO1 transcription factor instructs the germinal center dark zone program. *Immunity*. 43:1064–1074. https://doi.org/10.1016/j.immuni.2015.10.015

Fagarasan, S., S. Kawamoto, O. Kanagawa, and K. Suzuki. 2010. Adaptive immune regulation in the gut: T cell-dependent and T cell-independent IgA synthesis. *Annu. Rev. Immunol.* 28:243–273. https://doi.org/10.1146/annurev-immunol-030409-101314

Furukawa, K., A. Akasako-Furukawa, H. Shirai, H. Nakamura, and T. Azuma. 1999. Junctional amino acids determine the maturation pathway of an antibody. *Immunity*. 11:329–338. https://doi.org/10.1016/S1074-7613(00)80108-9

Gerner, M.Y., W. Kastenmuller, I. Ifrim, J. Kabat, and R.N. Germain. 2012. Histo-cytometry: a method for highly multiplex quantitative tissue imaging analysis applied to dendritic cell subset microanatomy in lymph nodes. *Immunity*. 37:364–376. https://doi.org/10.1016/j.immuni.2012.07.011

Gitlin, A.D., Z. Shulman, and M.C. Nussenzweig. 2014. Clonal selection in the germinal centre by regulated proliferation and hypermutation. *Nature*. 509:637–640. https://doi.org/10.1038/nature13300

Green, J.A., K. Suzuki, B. Cho, L.D. Willison, D. Palmer, C.D. Allen, T.H. Schmidt, Y. Xu, R.L. Proia, S.R. Coughlin, and J.G. Cyster. 2011. The

sphingosine 1-phosphate receptor $S1P_2$ maintains the homeostasis of germinal center B cells and promotes niche confinement. *Nat. Immunol.* 12:672–680. https://doi.org/10.1038/ni.2047

Inoue, T., R. Shinnakasu, W. Ise, C. Kawai, T. Egawa, and T. Kurosaki. 2017. The transcription factor Foxo1 controls germinal center B cell proliferation in response to T cell help. *J. Exp. Med.* 214:1181–1198. https://doi.org/10.1084/jem.20161263

Jarjour, M., A. Jorquera, I. Mondor, S. Wienert, P. Narang, M.C. Coles, F. Klauschen, and M. Bajénoff. 2014. Fate mapping reveals origin and dynamics of lymph node follicular dendritic cells. *J. Exp. Med.* 211: 1109–1122. https://doi.org/10.1084/jem.20132409

Luo, W., F. Weisel, and M.J. Shlomchik. 2018. B cell receptor and CD40 signaling are rewired for synergistic induction of the c-Myc transcription factor in germinal center B cells. *Immunity.* 48:313–326.e5. https://doi.org/10.1016/j.immuni.2018.01.008

Lycke, N.Y., and M. Bemark. 2017. The regulation of gut mucosal IgA B-cell responses: recent developments. *Mucosal Immunol.* 10:1361–1374. https://doi.org/10.1038/mi.2017.62

Nagashima, K., S. Sawa, T. Nitta, M. Tsutsumi, T. Okamura, J.M. Penninger, T. Nakashima, and H. Takayanagi. 2017. Identification of subepithelial mesenchymal cells that induce IgA and diversify gut microbiota. *Nat. Immunol.* 18:675–682. https://doi.org/10.1038/ni.3732

Naka, K., T. Hoshii, T. Muraguchi, Y. Tadokoro, T. Ooshio, Y. Kondo, S. Nakao, N. Motoyama, and A. Hirao. 2010. TGF-β-FOXO signalling maintains leukaemia-initiating cells in chronic myeloid leukaemia. *Nature.* 463:676–680. https://doi.org/10.1038/nature08734

Petritsch, C., H. Beug, A. Balmain, and M. Oft. 2000. TGF-β inhibits p70 S6 kinase via protein phosphatase 2A to induce $G(_1)$ arrest. *Genes Dev.* 14: 3093–3101. https://doi.org/10.1101/gad.854200

Radtke, A.J., W. Kastenmüller, D.A. Espinosa, M.Y. Gerner, S.W. Tse, P. Sinnis, R.N. Germain, F.P. Zavala, and I.A. Cockburn. 2015. Lymph-node resident $CD8\alpha^+$ dendritic cells capture antigens from migratory malaria sporozoites and induce $CD8^+$ T cell responses. *PLoS Pathog.* 11:e1004637. https://doi.org/10.1371/journal.ppat.1004637

Reboldi, A., and J.G. Cyster. 2016. Peyer's patches: organizing B-cell responses at the intestinal frontier. *Immunol. Rev.* 271:230–245. https://doi.org/10.1111/imr.12400

Reboldi, A., T.I. Arnon, L.B. Rodda, A. Atakilit, D. Sheppard, and J.G. Cyster. 2016. IgA production requires B cell interaction with subepithelial dendritic cells in Peyer's patches. *Science.* 352:aaf4822. https://doi.org/10.1126/science.aaf4822

Rodda, L.B., E. Lu, M.L. Bennett, C.L. Sokol, X. Wang, S.A. Luther, B.A. Barres, A.D. Luster, C.J. Ye, and J.G. Cyster. 2018. Single-cell RNA sequencing of lymph node stromal cells reveals niche-associated heterogeneity. *Immunity.* 48:1014–1028.e6. https://doi.org/10.1016/j.immuni.2018.04.006

Sander, S., V.T. Chu, T. Yasuda, A. Franklin, R. Graf, D.P. Calado, S. Li, K. Imami, M. Selbach, M. Di Virgilio, et al. 2015. PI3 kinase and FOXO1 transcription factor activity differentially control B cells in the germinal center light and dark zones. *Immunity.* 43:1075–1086. https://doi.org/10.1016/j.immuni.2015.10.021

Strasser, A., S. Whittingham, D.L. Vaux, M.L. Bath, J.M. Adams, S. Cory, and A.W. Harris. 1991. Enforced BCL2 expression in B-lymphoid cells prolongs antibody responses and elicits autoimmune disease. *Proc. Natl. Acad. Sci. USA.* 88:8661–8665. https://doi.org/10.1073/pnas.88.19.8661

Suzuki, K., M. Maruya, S. Kawamoto, K. Sitnik, H. Kitamura, W.W. Agace, and S. Fagarasan. 2010. The sensing of environmental stimuli by follicular dendritic cells promotes immunoglobulin A generation in the gut. *Immunity.* 33:71–83. https://doi.org/10.1016/j.immuni.2010.07.003

Travis, M.A., and D. Sheppard. 2014. TGF-β activation and function in immunity. *Annu. Rev. Immunol.* 32:51–82. https://doi.org/10.1146/annurev-immunol-032713-120257

Victora, G.D., and M.C. Nussenzweig. 2012. Germinal centers. *Annu. Rev. Immunol.* 30:429–457. https://doi.org/10.1146/annurev-immunol-020711-075032

Victora, G.D., T.A. Schwickert, D.R. Fooksman, A.O. Kamphorst, M. Meyer-Hermann, M.L. Dustin, and M.C. Nussenzweig. 2010. Germinal center dynamics revealed by multiphoton microscopy with a photoactivatable fluorescent reporter. *Cell.* 143:592–605. https://doi.org/10.1016/j.cell.2010.10.032

Wang, X., B. Cho, K. Suzuki, Y. Xu, J.A. Green, J. An, and J.G. Cyster. 2011. Follicular dendritic cells help establish follicle identity and promote B cell retention in germinal centers. *J. Exp. Med.* 208:2497–2510. https://doi.org/10.1084/jem.20111449

Wu, S., S.R. Majeed, T.M. Evans, M.D. Camus, N.M. Wong, Y. Schollmeier, M. Park, J.R. Muppidi, A. Reboldi, P. Parham, et al. 2016. Clathrin light chains' role in selective endocytosis influences antibody isotype switching. *Proc. Natl. Acad. Sci. USA.* 113:9816–9821. https://doi.org/10.1073/pnas.1611189113

Yadav, H., S. Devalaraja, S.T. Chung, and S.G. Rane. 2017. TGF-β1/Smad3 pathway targets PP2A-AMPK-FoxO1 signaling to regulate hepatic gluconeogenesis. *J. Biol. Chem.* 292:3420–3432. https://doi.org/10.1074/jbc.M116.764910

Yamazaki, S., A. Iwama, S. Takayanagi, K. Eto, H. Ema, and H. Nakauchi. 2009. TGF-β as a candidate bone marrow niche signal to induce hematopoietic stem cell hibernation. *Blood.* 113:1250–1256. https://doi.org/10.1182/blood-2008-04-146480

Yang, Y., C. Wang, Q. Yang, A.B. Kantor, H. Chu, E.E. Ghosn, G. Qin, S.K. Mazmanian, J. Han, and L.A. Herzenberg. 2015. Distinct mechanisms define murine B cell lineage immunoglobulin heavy chain (IgH) repertoires. *eLife.* 4:e09083. https://doi.org/10.7554/eLife.09083